Received 10 December 2015; revised 14 February 2016; accepted 24 February 2016. Date of publication 1 March 2016; date of current version 22 April 2016.
The review of this paper was arranged by Editor A. G. U. Perera.

Digital Object Identifier 10.1109/JEDS.2016.2536722

Photon Counting Error Rates in Single-Bit and Multi-Bit Quanta Image Sensors

ERIC R. FOSSUM (Fellow, IEEE)

Thayer School of Engineering, Dartmouth College, Hanover, NH 03755, USA

CORRESPONDING AUTHOR: E. R. FOSSUM (e-mail: eric.r.fossum@dartmouth.edu)

This work was supported by Rambus Inc.

ABSTRACT Photon or photoelectron counting error (bit error) rates are determined for single-bit and multi-bit quanta image sensors (QISs). The results are also applicable to CMOS image sensors with deep sub-electron read noise. The effects of read noise, gain variation, and quanta exposure level on the counting errors (bit errors) in a QIS device are investigated. The interaction of these factors yields complex behavior of the counting error rate. Still, photon-counting is predicted to be remarkably accurate for quanta exposures greater than unity despite read noise and conversion-gain variation, and accurate at very low-light levels if the read noise is less than 0.15e- r.m.s.

INDEX TERMS CMOS image sensor, quanta image sensor, jot device, photon counting, high conversion gain, low read noise, low dark current, single photon detectors.

I. INTRODUCTION

The Quanta Image Sensor (QIS) is a CMOS image sensor containing a large number of specialized sub-diffraction-limit-sized pixels with deep sub-electron read noise (less than 0.5e- r.m.s.) that allows photoelectron counting (or photon counting if quantum efficiency is sufficiently high.) The specialized pixel is referred to as a jot, and the output of multiple jots are combined to create a gray-scale image pixel. The full-well capacity of the jots is typically small, less than a few hundred electrons, due to a combination of small storage-well capacity, high conversion gain, low voltage operation, and limited analog-to-digital converter (ADC) bit depth. The QIS concept, first introduced in 2005 [1], [2], has evolved from single-bit operation to also include multi-bit operation. Imaging performance of the QIS has been analyzed for signal and noise as a function of quanta exposure H, the average number of photoelectrons, as well as for high dynamic range operation due to the QIS' inherent non-linearity as H approaches the full-well capacity of the sensor [3], [4].

Significant progress has been made towards the practical implementation of a QIS for both the jot device and readout electronics. A pump-gate jot was fabricated in a 65nm commercial CMOS image sensor (CIS) backside-illuminated (BSI) process with 1.4μm jot pitch, and shown to exhibit deep sub-electron read noise as low as 0.22e- r.m.s. with conversion gain (CG) as high as 423μV/e-. The pump-gate jot exhibited photoelectron-counting capability with reasonable accuracy without the use of avalanche gain or low-temperature multiple-sample operation [5]–[7]. A 1Mpixel 1000fps binary image sensor was demonstrated with total power dissipation of less than 20mW including pads, and a figure of merit of 2.5pJ/bit [8]. A combination of the deep-sub-electron jot with low-power, high-speed readout has not yet been demonstrated but no significant hurdles for successful implementation are believed to remain.

In the pump-gate jot test devices, CG variation (standard deviation normalized to the mean) of the order of 2-3% was observed. CG variation is a form of photo-response non-uniformity (PRNU) that arises from the sense node capacitance of the jot. Variation in ADC quantizer thresholds in the multi-bit QIS can potentially result in a similar effect. PRNU in state-of-the-art CMOS image sensors is less than 2%, and it is likely that through product engineering, CG variation in jot devices will also drop below the 2% range. However, the observed CG variation raised questions about the relationship between CG variation and photon-counting errors, which is similar to issues of PRNU in conventional CIS. However, for PRNU in consumer applications, it is the

visual aesthetics that are of concern, whereas for quantitative photon-counting applications, analysis of count error rates as a function of operating conditions and device parameters such as CG variation and read noise is important for understanding and predicting instrument performance.

In this paper, photoelectron (or photon) counting error rates are assessed as a function of read noise, conversion gain variation and quanta exposure. Other sources of error including dark count rate (a.k.a. dark current), optical crosstalk including color information, and electronic crosstalk, are not considered here. The results provide a means for assessing the accuracy of QIS-based photon-counting instrumentation and systems in the future, and will help guide their development, as well as inform future investigators about the performance accuracy of such systems. The results are also applicable to other emerging deep sub-electron read noise image sensors intended for photon-counting applications (e.g., [9] and [10]).

II. READOUT VOLTAGE PROBABILITY DENSITY FUNCTION

In the QIS, the voltage that is readout from the pixels or jots contains information about the number of collected electrons and the conversion gain of the jot. The number of electrons depends on the number of incident photons, the quantum efficiency, and carrier collection efficiency, among other factors. There is a natural fluctuation in the number of incident photons, carrier generation rate and carrier collection efficiency resulting in a fluctuation in readout voltage from readout to readout of the same jot for the same average photon flux. The net fluctuation or "shot noise" is well-described by Poisson statistics.

Voltage-referred noise is also added during the readout process. This could come from avalanche-gain variation in avalanche-based devices such as single-photon avalanche detectors (SPADs), or from current variations in the in-pixel readout transistor, often a source-follower MOSFET. The latter noise is typically dominated by 1/f noise and thermal noise not fully removed by noise-shaping during the correlated double-sampling readout process [11]. Additional noise may arise in downstream electronics and analog-to-digital conversion, but with enough voltage gain early in the signal chain, these noise sources are often inconsequential.

When imaging a static scene with a QIS jot, the device receives an average of H photoelectrons during the integration period. The probabilities $\mathbb{P}[k]$ of receiving k photoelectrons are given by the Poisson probability mass function:

$$\mathbb{P}[k] = \frac{e^{-H}H^k}{k!} \tag{1}$$

During readout, the photoelectron signal from the jot is both converted to a voltage and corrupted by noise. Let CG be the conversion gain (V/e-) for the jot and let the uncorrupted voltage signal from the jot be given by $V_{sig} = CG \cdot k$. It is convenient to normalize the voltage signal to electrons, so

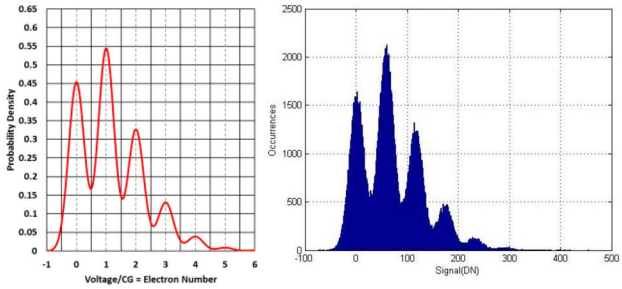

FIGURE 1. Readout signal probability as a function of normalized voltage (electron number) as calculated from Eq. 6 using u_n=0.265 e- r.m.s. and H=1.2 (left), and experimental histogram data (right).

let the normalized uncorrupted signal U_{sig} be defined by:

$$U_{sig} \triangleq \frac{V_{sig}}{CG} \tag{2}$$

Thus, the value of $U_{sig} \in \{0, 1, 2, 3 \text{ etc.}\}$ depends on the number of photoelectrons read out, and is also referred to as the electron number. The probability that the electron number U_{sig} is equal to k is given by $\mathbb{P}[k]$ from Eq. 1. In the absence of read noise, the uncorrupted readout voltage probability density function (ROVPDF) for reading out signal U_{sig} from the jot, $P[U_{sig}]$, is a series of Dirac delta functions:

$$P[U_{sig}] = \sum_{k=0}^{\infty} \delta(U_{sig} - k) \cdot \mathbb{P}[k] \tag{3}$$

Let the additive r.m.s. voltage noise after conversion and before analog-to-digital quantization (e.g., source-follower 1/f and thermal noise) be given by v_n. Let the normalized noise u_n be defined by:

$$u_n \triangleq \frac{v_n}{CG} \tag{4}$$

If the read noise is described by a normal distribution, then the component PDF $P[U]$ for reading the corrupted signal U is given by:

$$P[U] = \frac{1}{\sqrt{2\pi u_n^2}} exp\left[-\frac{(U - U_{sig})^2}{2u_n^2}\right] \tag{5}$$

For a given quanta exposure, the ROVPDF depends both on the probability of collecting k photoelectrons and on the read noise, and is given by:

$$P[U] = \sum_{k=0}^{\infty} \frac{\mathbb{P}[k]}{\sqrt{2\pi u_n^2}} exp\left[-\frac{(U - k)^2}{2u_n^2}\right] \tag{6}$$

Essentially, the ROVPDF is a convolution of the Poisson distribution for quanta exposure H (Eq. 3) and a normal distribution with read noise u_n (Eq. 5) and the result is a sum of constituent PDF components, one for each possible value of k and weighted by the Poisson probability for that k. An example comparing the ROVPDF to an experimental photon-counting histogram (PCH) is shown in Fig. 1 (obtained like those shown in [6] and [7]) and generally good agreement

has been found between this model and experiments. The peak spacing reflects electron quantization and can be used to determine conversion gain. The distribution and amplitude of peaks reflects the Poisson distribution, and the valley-to-peak modulation (VPM) of the experimental histogram can be used to determine read noise for the device under test [6], [7], [12].

In a practical implementation of a QIS, conversion gain may vary from jot to jot due to variations in sense node capacitance, in turn due to random variations in feature dimensions or implant concentrations. In the case of a QIS using pump-gate jots or related devices, conversion gain variation comes from variation of the capacitance of the floating diffusion node, with voltage noise subsequently added by the source-follower transistor. In this case, the voltage noise V_n is generally independent of variation in CG [7]. In other photodetector devices the voltage noise V_n may be a function of CG and electron number k.

If there is a jot with a different conversion gain $CG' = CG + \Delta CG$, there is a shift in the peak positions of the ROVPDF. The ROVPDF of Eq. 6 becomes:

$$P[U] = \sum_{k=0}^{\infty} \frac{\mathbb{P}[k]}{\sqrt{2\pi u_n^2}} exp\left[-\frac{(U-(1+\gamma)k)^2}{2u_n^2}\right] \tag{7}$$

where $\gamma \triangleq \Delta CG/CG \ll 1$.

Consider an ensemble of jots (e.g., the jots in a QIS array) that has a mean conversion gain $\overline{CG}$ and CG variance σ_{CG}^2 where $\sigma_{CG}/\overline{CG} \ll 1$. If each jot receives k photoelectrons, the jots have a mean signal $\bar{V}_{sig} = \overline{CG} \cdot k$, and the ROVPDF for the ensemble without read noise is given by:

$$P[V] = \frac{1}{k\sigma_{CG}\sqrt{2\pi}} exp\left[-\frac{\left(V-\bar{V}_{sig}\right)^2}{2(k\sigma_{CG})^2}\right] \tag{8}$$

and in terms of the normalized readout voltage U,

$$P[U] = \frac{1}{\left(k\sigma_{CG}/\overline{CG}\right)\sqrt{2\pi}} exp\left[-\frac{\left(U-\bar{U}_{sig}\right)^2}{2\left(k\sigma_{CG}/\overline{CG}\right)^2}\right] \tag{9}$$

where $\sigma_{CG}/\overline{CG}$ is a fraction similar to γ above.

To include the effects of CG variation on the ROVPDF of Eq. 6, we must convolve the two distributions. This leads to the combined ROVPDF:

$$P[U] = \sum_{k=0}^{\infty} \frac{\mathbb{P}[k]}{\sqrt{2\pi\sigma_k^2}} exp\left[-\frac{(U-k)^2}{2\sigma_k^2}\right] \tag{10}$$

where

$$\sigma_k \triangleq \sqrt{u_n^2 + \left(k\sigma_{CG}/\overline{CG}\right)^2} \tag{11}$$

and σ_k can be considered a combination of temporal read noise and PRNU "noise", the latter of which is dependent on the electron number k. For example, a 5% CG variation will lead to PRNU noise comparable to 0.30e- r.m.s. read noise for k=6e-.

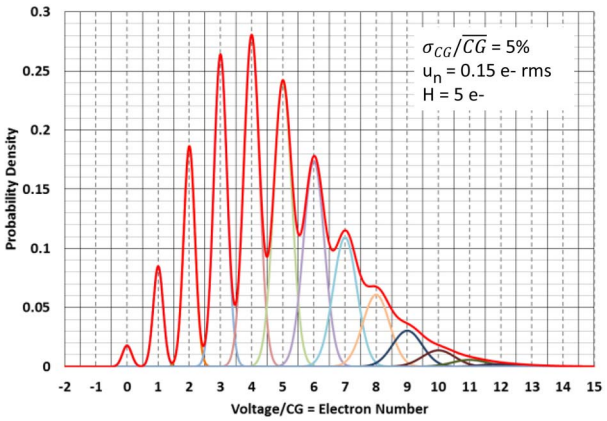

FIGURE 2. Readout signal probability (ROVPDF) for H=5.0, read noise of 0.15e- r.m.s., and conversion gain variation of 5% in red. Constituent PDFs shown for reference in other colors.

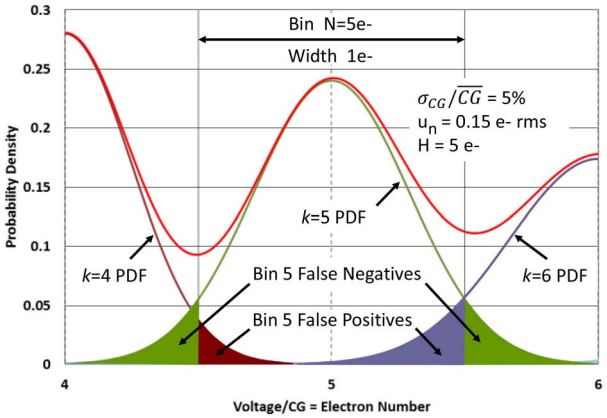

FIGURE 3. Readout signal probability (ROVPDF) for H=5.0, read noise of 0.15e- r.m.s., and conversion gain variation of 5%, centered on Bin N=5e-. Constituent PDFs for k=4, 5 and 6 shown in dark red, green and purple, respectively.

An example of the combined ROVPDF is shown in Fig. 2, along with the component PDFs. The increasing width of the component PDFs with electron number due to CG variation results in reduced ROVPDF valley-peak modulation with electron number, to the point where the peaks nearly vanish at higher electron numbers in this example. Similar PCH features have been observed in SPAD devices [13], [14] and perhaps CG variation (avalanche gain variation) is a factor in those cases [15]. It can also be observed that using peak heights alone could lead to an erroneous estimation of the quanta exposure. From the ROVPDF peak heights seen in Fig 2, which reflect the Poisson distribution, one might underestimate the quanta exposure H to be 4.4 rather than 5.0 due to the distortion in peak heights. Quanta exposure calculated using the full distribution yields the proper value of $H = 5.0$. The VPM technique, when applied to Fig. 2 for the valley at U=5.5, yields a value of σ_k=0.32e- r.m.s., which is what is expected for u_n=0.15e- r.m.s., $\sigma_{CG}/\overline{CG}$=5%, and k=5.5 in Eq. 11.

III. COUNTS IN BINS

In an n-bit multi-bit QIS, the jot signal is quantized by an n-bit analog-to-digital converter (ADC) with 2^n quantization levels, where each count of the converter corresponds to one electron. Thus, a 3b QIS would have 8 quantization levels corresponding to 0, 1, 2, 3, 4, 5, 6, and 7 electrons, and would saturate at 7e- digital output for higher signal levels. To quantize these values, the ADC would divide the signal voltage range into 8 bins with 7 bin boundaries at electron numbers of 0.5, 1.5, 2.5, up to 6.5e- (e.g., solid vertical lines of Fig. 1). We label these bins with bin numbers $N \in \{0, 1, 2, 3, 4, 5, 6, 7\}$. The bin number N is also referred to as the electron number.[1]

Ideally, a signal corresponding to k electrons would result in a count in bin $N=k$. However, due to noise, there is a probability that a signal of k electrons is quantized as a count in bin $N<k$ or $N>k$. The probability of misquantization can be visualized using the ROVPDF as shown in Fig. 3, which shows the constituent PDF elements of the ROVPDF. These are the $k=4$, $k=5$ and $k=6$ PDFs broadened by the noise σ_k. Some of the $k=5$ PDF spills into adjacent bins $N=4$ and $N=6$, reducing the count in bin $N=5$ due to the $k=5$ PDF (false negatives) and increasing the count in the adjacent bins (false positives for those bins). Similarly, the count in bin $N=5$ is increased by "contamination" from the $k=4$ and $k=6$ PDFs. The false positive contamination that causes count error in the bin depends on the noise σ_k, which in turn depends on k, as well as the amplitudes of the constituent distributions that are determined by the quanta exposure and electron number.

Henceforth, the count in a bin is defined as the integral of the ROVPDF within the bin boundaries, so that the total count, as an unweighted sum from all bins, is unity. The ideal count in bin N is given by $\mathbb{P}[N]$, the Poisson probability mass function value for $k=N$. The expected count of a bin in practice would be the count calculated here multiplied by the total number of signal samples taken. To count the number of electrons, one takes a sum of the count in each bin, weighted by the bin number N (see Eq. 18).

To calculate the error, it is useful to calculate the integral $\Phi(a, b)$ of a normal distribution P[x] with mean $\bar{x}$ and variance σ^2, over the range (a<x<b) as:

$$\Phi(a,b) = \frac{1}{2}\left[\mathrm{erf}\left(\frac{b-\bar{x}}{\sigma\sqrt{2}}\right) - \mathrm{erf}\left(\frac{a-\bar{x}}{\sigma\sqrt{2}}\right)\right] \tag{12}$$

The count contribution to bin N, with boundaries $N-\frac{1}{2}$ to $N+\frac{1}{2}$, from the PDF corresponding to electron number k, is thus

$$C_{N,k} = \frac{1}{2}\mathbb{P}[k]\left[\mathrm{erf}\left(\frac{N+\frac{1}{2}-k}{\sigma_k\sqrt{2}}\right) - \mathrm{erf}\left(\frac{N-\frac{1}{2}-k}{\sigma_k\sqrt{2}}\right)\right] \tag{13}$$

1. The number of photoelectrons, k, and its associated voltage signal U_{sig}, are "internal" QIS values, and the bin electron number N is a measured signal from quantizer in the QIS.

And the total count C_N in bin N from all constituent PDFs is given by:

$$C_N = \sum_{k=0}^{\infty} C_{N,k} \tag{14}$$

For $\sigma_k \lesssim 0.50$e- r.m.s., only adjacent constituent PDFs need be considered since other addends are insignificant.

$$C_N \cong \sum_{k=N-1}^{N+1} C_{N,k} \tag{15}$$

The counts in bin 0 and in the last bin $N_L=2^n$-1, are calculated slightly differently. Bin 0 includes all contributions below the boundary at electron number 0.5 and we must use $\Phi(-\infty, b)$ yielding

$$C_0 = \frac{1}{2}\sum_{k=0}^{\infty}\mathbb{P}[k]\left[\mathrm{erf}\left(\frac{\frac{1}{2}-k}{\sigma_k\sqrt{2}}\right)+1\right] \tag{16}$$

Likewise, for the last bin N_L we must use $\Phi(a, +\infty)$ yielding

$$C_{N_L} = \frac{1}{2}\sum_{k=0}^{\infty}\mathbb{P}[k]\left[1-\mathrm{erf}\left(\frac{(2^n-1)-\frac{1}{2}-k}{\sigma_k\sqrt{2}}\right)\right] \tag{17}$$

The total number of photoelectrons counted in each bin, N_{TOT}, is just

$$N_{TOT} = \sum_{N=0}^{\infty} N \cdot C_N \tag{18}$$

In practice, the readout of a multibit jot yields just one ADC value, ranging from 0 to 2^n-1. Only when many jots are read out, either from different spatial locations different fields, or some combination, can a histogram or ROVPDF be formed, and the "noise" in the experimental data histogram is only smoothed when thousands of read out jots are included, as was the case for the histogram shown in Fig. 1.

IV. COUNTING ERRORS

In the context of photon counting or photoelectron counting, a definition of a count error is needed. A count error is an error in the expected value of the count in a bin, or of the total number of electrons counted by one jot over many integration periods, or of the total electrons counted by an ensemble of jots, or some combination of the three.

Bin errors are the easiest to quantify. As stated earlier, the ideal count in a bin should be the Poisson probability mass function value for the electron count corresponding to that bin number. For example, for $H=5$, the count in bin $N=5$ should be approximately 17.55% of the total number of signals measured. If we sampled a steady illumination 200,000 times with a single jot, the readout of that jot ideally would yield 5 electrons (a count in bin 5) for 35,100 of the readouts, with lower counts for the other bins (except bin 4 which should yield the same result as bin 5 in this case). In fact, the exposure H might be determined from just the

relative count values of a few bins. (This is not the same as determining H from relative peak values of the PCH [12].)

The difference between the expected count determined by read noise and/or PRNU noise and the ideal count in a particular bin, is an error. When the error is normalized by the ideal count, we call this the Poisson error rate (PER).

$$PER\,(N) = \frac{\{C_N - \mathbb{P}\,[N]\}}{\mathbb{P}\,[N]} = \frac{C_N}{\mathbb{P}\,[N]} - 1 \tag{19}$$

Note that this rate metric can yield large values when C_N and $\mathbb{P}\,[N]$ are both small and, in reality, inconsequential.

Alternatively, one can use a more classical bit (or bin) error rate (BER) definition, where errors are the contributions to bin N that do not originate from the k=N PDF, normalized by the ideal count. These are false positive counts. Subtracting the k=N term from Eq. 14 yields:

$$BER\,(N) = \frac{\left\{C_N - \mathbb{P}\,[N]\,\mathrm{erf}\left(\frac{1}{\sigma_k\sqrt{8}}\right)\right\}}{\mathbb{P}\,[N]} \tag{20}$$

or

$$BER\,(N) = PER\,(N) + \mathrm{erfc}\left(\frac{1}{\sigma_k\sqrt{8}}\right) \tag{21}$$

This rate metric has similar limitations as Eq. 19, where the BER may be artificially high, but if the actual count is close to zero, the BER is inconsequential for photon-counting applications. One might also consider including false-negative contributions, that is, counts from the k=N PDF that fall outside bin N. Strictly speaking these are also errors, but are already accounted for as false positives in adjacent bins.

One might also consider the total error rate for all bins.

$$PER_T = \sum_{N=0}^{2^n-1} PER(N) \tag{22}$$

or

$$BER_T = \sum_{N=0}^{2^n-1} BER(N) \tag{23}$$

For example, for a single-bit QIS, and considering contamination only from adjacent distributions, one obtains the single-bit BER_T:

$$BER_T = \frac{1}{2}erfc\left[\frac{1}{u_n\sqrt{8}}\right](1+H)e^{-H} \tag{24}$$

This is plotted in Fig. 4. The single-bit BER_T assessed in [3] did not include the effect of the Poisson distribution, and is thus only valid for $H \lesssim 0.1$.

The total error rate can include positive and negative contributions that partially cancel each other out, leading to a lower total error rate than that in the individual bins.

One issue with the total error rate calculation comes from the count in the last bin, N_L=2^n-1. This bin includes counts in "larger" bins since the n-bit quantizer saturates at this level, which leads to the non-linear compressive behavior of the single-bit and multi-bit QIS at higher exposures. Thus, relative to the ideal Poisson count, the total error rate climbs to 100% as the non-linear behavior grows.

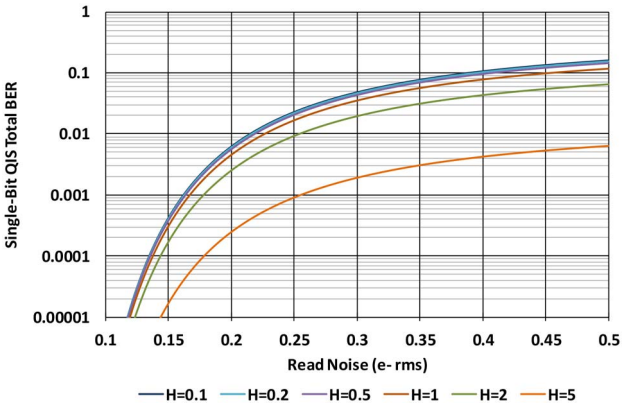

FIGURE 4. Total BER for a single-bit QIS as a function of read noise and for different quanta exposure levels (H).

Of related interest is the count error rate for the case of a single jot with conversion gain variation as described by the ROVPDF of Eq. 7. In this case, the shift in the ROVPDF peak position increases the contamination of constituent PDFs in forward neighboring bins (for positive γ). This is particularly acute in the vicinity of $H \approx N \approx \frac{1}{2\gamma}$ where the shift moves a constituent PDF peak to the edge of the bin and causes significant dips in C_N. Assuming adjacent bin contamination only ($u_n \lesssim 0.5$), the total error rate for a single jot with conversion gain variation γ can be expressed as:

$$BER_T = \frac{1}{2}\sum_{N=0}^{2^n-2}\mathbb{P}[k]erfc\left[\frac{1-2\gamma N}{\sqrt{8}\;u_n}\right] + \frac{1}{2}\sum_{N=1}^{2^n-1}\mathbb{P}[k]erfc\left[\frac{1+2\gamma N}{\sqrt{8}\;u_n}\right] \tag{25}$$

Example calculations of the error rate were shown in [7]. Another example of BER and PER as a function of bin number N or electron number k are shown in Fig. 5 for read noise of 0.15e- r.m.s., quanta exposure level H=5 and different conversion gain variations. Also shown is a constant 5% error rate for reference. PER is generally lower than BER since some positive and negative counting errors can cancel. The absolute value of PER is plotted, and the dips reflect PER sign changes.

While interesting to contemplate, numerical calculation of these bin-wise and total PERs and BERs for a variety of conditions has, regrettably, led to little insight into the performance capability of the QIS.

V. EFFECT OF COUNTING ERRORS ON THE RESPONSE CURVE

For most anticipated QIS applications, an ensemble of jots will be read out, and the number of photoelectrons collected

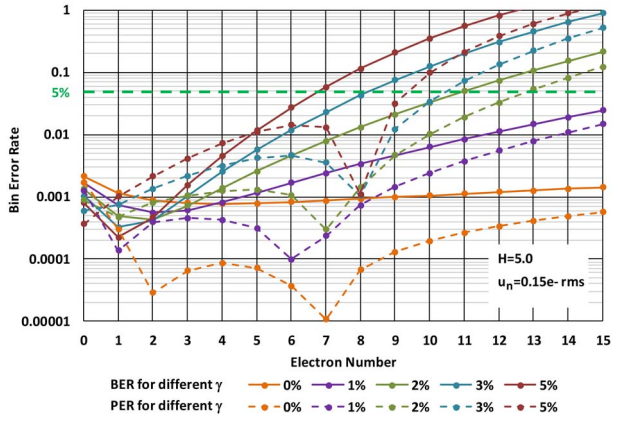

FIGURE 5. Single-jot bit error rate (BER) and Poisson error rate (PER) as a function of bin or electron number for different conversion gain variations γ (shown as percentage in legend) with H=5.0 and read noise of 0.15e- r.m.s.. Green dashed line shows 5% error, for reference.

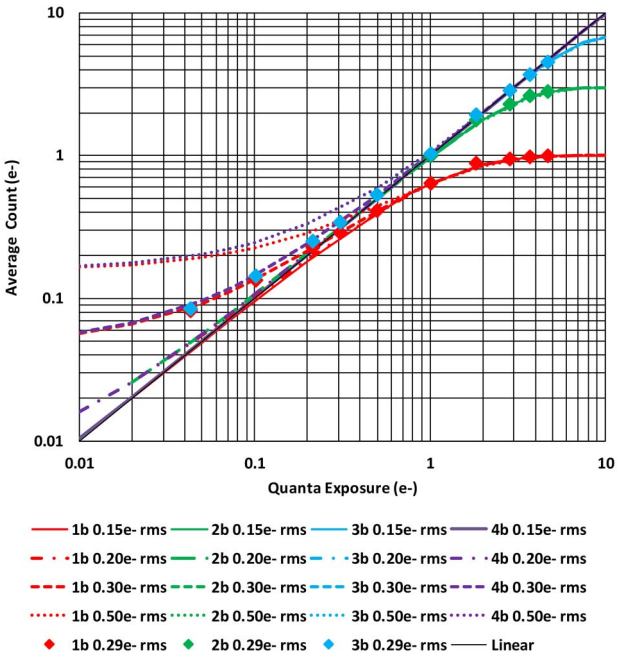

FIGURE 6. Expected response of single-bit and multi-bit QIS as a function of bit depth and read noise. Impact of conversion gain variation up to 20% is negligible. Experimental data is shown by diamond symbols.

for each of the jots will be measured using an on-chip quantizer (ADC). The measured quantities will be subject to "shot noise" as a manifestation of the Poisson statistics, but assuming the jots are all subject to the same quanta exposure H, there will be a measurement of the mean that should be equal to the theoretical response curves calculated in [3]. These results reflect the performance of an ideal QIS, with no read noise, uniform jot performance, perfect quantizer, etc.

The expected response of the ideal QIS (e.g., the average response of a large ensemble of jots and n-bit quantizer) is an S-shaped D-log H curve, like that of photographic film [2], [3]. The response for low quanta exposures (H<0.1 for single bit QIS, H<1 for multi-bit QIS) is quite linear, with increased non-linearity for increasing quanta exposure asymptotically reaching the full well capacity of 2^n-1, as limited by the quantizer bit depth. The extent of the non-linear region is reduced with increasing bit depth [3], [4].

The response of the QIS was calculated using the expected count in each bin from Eqs. 14-17, as shown in Fig. 6 for various read noise levels and bit-depths, but with no conversion gain variation. For low quanta exposures, such as those important for many scientific applications, the impact of 0.15e- r.m.s. read noise is minimal, at least for H down to 0.01, but increases with noise. In this low light region most counts are zero with few true positive counts as reflected by H. However, with increasing noise, the chance that the absence of a photoelectron, when combined with additive read noise, is erroneously counted as a positive also increases.

Consider H=0.01, that is, one photoelectron expected for every 100 reads. At 0.20e- r.m.s. read noise, the expected readout count is 0.016, or 60% more than the ideal count. By 0.3e- r.m.s., the expected count rises to 0.056, or a 460% error. At H=0.10, the impact of 0.20e- r.m.s. read noise is negligible, but 0.30e- r.m.s. read noise still leads to a 34% error. The errors in this low quanta exposure range are nearly independent of bit depth because most of the counts are in bin 0, with only a few in bin 1. Higher bins have negligible counts for low quanta exposures.

At higher quanta exposures (H>1) the impact of read noise on count error compared to the ideal QIS response is minimal and the non-linear behavior is as expected.

The experimental device data collected in [7] using a fine-resolution, off-chip ADC was reprocessed to emulate quantization into bins using a coarser ADC. Single-bit, 2-bit and 3-bit depths were emulated. The read noise of the data was estimated to be 0.29e- r.m.s. by the VPM method also described in [6]. The data agrees well with the theory, and in fact it was the divergence from ideal behavior at low quanta exposure levels that motivated some of the analysis in this paper.

The effect of conversion gain variation on the response curves was also modelled. Based on the strong impact of CG variation on a single jot's BER described previously, the expectation was that CG variation would have a significant negative impact on the expected response of an ensemble of jots with CG variation. In fact, the response is hardly measureable, both for low and higher quanta exposure levels, and modelling CG variation as high as 20% gave rise to response curves indistinguishable from those of Fig 6.

At low quanta exposure levels most counts are in bin 0 or bin 1. CG variation has little impact on the quantization of signal in this range, just as the case for a single jot with CG variation. At higher quanta exposure levels, any single jot's total count of photoelectrons is proportional to its CG variation. That is, if the CG is 5% higher, the count also increases by approximately 5% as one might expect. However, with a large ensemble, and assuming a normal distribution of CG

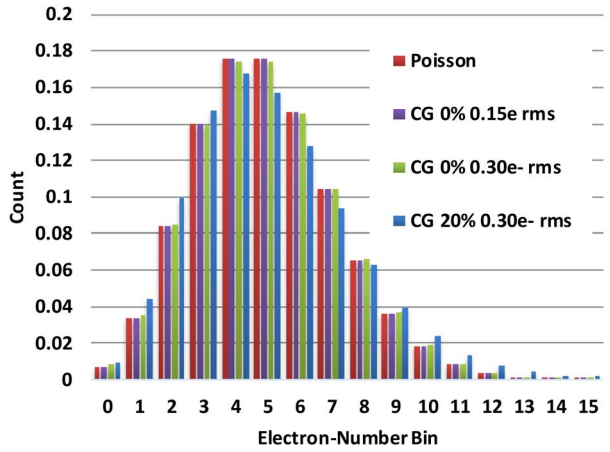

FIGURE 7. Expected count histogram as a function of electron-number bin for different read noise and CG variation levels for quanta exposure H=5, compared to ideal Poisson values.

variation, for each jot that is over counting, there is another jot that is undercounting, and on average their errors cancel.

In Fig. 7, a histogram of expected counts in different quantizer bins is shown, with each bin corresponding to one electron number, for a quanta exposure H=5. This exposure was chosen just for illustrative purposes. The Poisson probability mass function is shown by the first column and represents the ideal count. Also shown are columns corresponding to read noise of 0.15e- r.m.s. with no CG variation, read noise of 0.30e- r.m.s. with no CG variation, and read noise of 0.30e- r.m.s. with 20% CG variation, respectively. In the latter case, the variation is set high for illustrative purposes, and it is seen that the count is above the Poisson ideal count in lower and higher bins, and below the Poisson ideal level in the central bins. Yet, the total expected photoelectron count ranges between 4.9985 and 5.0002 for each case, despite the very high CG variation and concomitant distortion from the ideal count histogram. This total count accuracy corresponds to the indistinguishable data at H=5 on the 4b QIS curve in Fig. 6.

CG variation will of course give rise to PRNU with jots just as it does with CIS pixels, and in a small patch of uniformly exposed jots, CG variation will give rise to spatial PRNU noise. Unlike CIS pixels though, most image formation algorithms will use a spatial kernel of jots to create an image pixel, so that there will be improved PRNU due to the effective spatial averaging of individual jot responses.

VI. CONCLUSION

In this paper the effect of read noise, Poisson statistics, gain variation and quanta exposure on photon-counting (or bit) error rates for single-bit and multi-bit QIS devices was investigated. The results are also applicable to all CMOS image sensors with deep sub-electron read noise. Generally, as expected, bit error rate increases for higher read noise (wider peaks in the distribution) and higher conversion gain variation.

Two types of counting errors were considered. The conventional bit error rate is determined from counting false positives in each bin. The Poisson error rate was defined as the error compared to what is expected from Poisson statistics. In this case, false positives can be compensated by false negatives and the Poisson error rate is generally less than the conventional bit error rate. The bin-wise bit-error rate increases for higher electron numbers and for higher conversion gain variation. Both error rates depend on exposure level yielding somewhat complex behavior.

The single-bit QIS is minimally impacted by conversion gain variation as would be expected, since one is only interested in comparisons to a single 0.5e- threshold level. In multi-bit devices, gain variation is reflected in higher bit error rates in higher bin numbers. The science impact of such errors may, in practice, be smaller for higher electron numbers since the percentage error (e.g., 1 out of 14) is smaller, and shot noise also grows with higher electron number. That is, a quantization error between 14e- and 15e- a few percent of the time may be less important in many applications, than say between 1e- and 2e-.

The total count error was also examined and it was found that conversion gain variation, when described by a (symmetric) normal distribution, has little effect on total count error both for low light levels and higher light levels. Read noise also has little effect on total count error for higher light levels, but can cause significant systematic error at low light levels, since false positives from read noise can artificially increase the count. Generally, the read noise needs to be less than 0.15e- r.m.s. at low light levels ($0.01<H<1.0$) to obtain accurate photoelectron counting. Accurate counting for lower quanta exposure levels ($H<0.01$) may require even lower read noise.

The accuracy of photon-counting predicted by this work in the presence of read noise and conversion gain variation at higher light levels exceeded the author's expectations at the onset of the investigation. Some effort was required to believe and understand the results of this modeling. Also of surprise was the strong deleterious effect of read noise of just 0.3e- r.m.s. on photon-counting accuracy for very low light levels, counter to prior guidance [16], [17], leading to further conviction that accurate photon-counting image sensors require read noise of 0.15e- r.m.s or less [3].

ACKNOWLEDGMENT

The author appreciates discussion with his graduate students, particularly J. J. Ma for taking the experimental data, and D. Starkey for proof-reading, and his colleague Prof. K. Odame. A discussion with Prof. M. Borsuk that lead to an improved understanding of the predicted accuracy is particularly appreciated.

REFERENCES

[1] E. R. Fossum, "Some thoughts on future digital still cameras," in *Image Sensors and Signal Processing for Digital Still Cameras*, J. Nakamura, Ed. Boca Raton, FL, USA: CRC Press, 2005, pp. 305–314.

[2] E. R. Fossum, "What to do with sub-diffraction-limit (SDL) pixels? A proposal for a gigapixel digital film sensor (DFS)," in *Proc. IEEE Workshop Charge Coupled Devices Adv. Image Sensors*, Karuizawa, Japan, Jun. 2005, pp. 1–4.
[3] E. R. Fossum, "Modeling the performance of single-bit and multi-bit quanta image sensors," *IEEE J. Electron Devices Soc.*, vol. 1, no. 9, pp. 166–174, Sep. 2013.
[4] E. R. Fossum, "Multi-bit quanta image sensors," in *Proc. Int. Image Sensor Workshop*, Vaals, The Netherlands, Jun. 2015. [Online]. Available: http://www.imagesensors.org/Past%20Workshops/2015%20Workshop/2015%20Papers/Sessions/Session_9/9-03_Fossum.pdf
[5] J. Ma and E. R. Fossum, "A pump-gate jot device with high conversion gain for a quanta image sensor," *IEEE J. Electron Devices Soc.*, vol. 3, no. 2, pp. 73–77, Mar. 2015.
[6] J. Ma and E. R. Fossum, "Quanta image sensor jot with sub 0.3e- r.m.s. read noise," *IEEE Electron Device Lett.*, vol. 36, no. 9, pp. 926–928, Sep. 2015.
[7] J. Ma, D. Starkey, A. Rao, K. Odame, and E. R. Fossum, "Characterization of quanta image sensor pump-gate jots with deep sub-electron read noise," *IEEE J. Electron Devices Soc.*, vol. 3, no. 6, pp. 472–480, Nov. 2015.
[8] S. Masoodian, A. Rao, J. Ma, K. Odame, and E. R. Fossum, "A 2.5 pJ/b binary image sensor as a pathfinder for quanta image sensors," *IEEE Trans. Electron Devices*, vol. 63, no. 1, pp. 100–105, Jan. 2016. [Online]. Available: http://ieeexplore.ieee.org/stamp/stamp.jsp?tp=&arnumber=7172527.
[9] M.-W. Seo, S. Kawahito, K. Kagawa, and K. Yasutomi, "A 0.27e- rms read noise 200-uV/e- conversion gain reset-gate-less CMOS image sensor with 0.11-um CIS process," *IEEE Electron Dev. Lett.*, vol. 36, no. 12, pp. 1344–1347, Dec. 2015.
[10] J. R. Janesick, T. Elliott, J. Andrews, J. Tower, and J. Pinter, "Fundamental performance differences of CMOS and CCD imagers: Part VI," in *Proc. SPIE*, vol. 9591. San Diego, CA, USA, Aug. 2015, Art. no. 959102, doi: 10.1117/12.2189941.
[11] R. J. Kansy, "Response of a correlated double sampling circuit to 1/f noise [generated in CCD arrays]," *IEEE J. Solid-State Circuits*, vol. 15, no. 3, pp. 373–375, Jun. 1980.
[12] D. Starkey and E. R. Fossum, "Determining conversion gain and read noise using a photon-counting histogram method for deep sub-electron read noise image sensors," *IEEE J. Electron Devices Soc.*, to be published, doi: 10.1109/JEDS.2016.2536719.
[13] L. Gasparini, N. Massari, M. Perenzoni, L. Pancheri, and D. Stoppa, "Compact time-gated analog counting SPAD-based pixels for high resolution, single-photon, time-resolved imagers," in *Proc. Int. Image Sensor Workshop*, Vaals, The Netherlands, Jun. 2015. [Online]. Available: http://www.imagesensors.org/Past%20Workshops/2015%20Workshop/2015%20Papers/Sessions/Session_7-Posters2/7-17_Gasparini.pdf
[14] N. A. W. Dutton *et al.*, "A SPAD-based QVGA image sensor for single-photon counting and quanta imaging," *IEEE Trans. Electron Devices*, vol. 63, no. 1, pp. 189–196, Jan. 2016, doi: 10.1109/TED.2015.2464682.
[15] V. Savuskan, I. Brouk, M. Javitt, and Y. Nemirovsky, "An estimation of single photon avalanche diode (SPAD) photon detection efficiency (PDE) nonuniformity," *IEEE Sensors J.*, vol. 13, no. 5, pp. 1637–1640, May 2013.
[16] N. Teranishi, "Required conditions for photon-counting image sensors," *IEEE Trans. Electron Devices*, vol. 59, no. 8, pp. 2199–2205 Aug. 2012.
[17] Q. Yao, B. Dierickx, B. Dupont, and G. Ruttens, "CMOS image sensor reaching 0.34 e-rms read noise by inversion-accumulation cycling," in *Proc. Int. Image Sensor Workshop*, Vaals, The Netherlands, Jun. 2015. [Online]. Available: http://www.imagesensors.org/Past%20Workshops/2015%20Workshop/2015%20Papers/Sessions/Session_12/12-04_Yao.pdf

ERIC R. FOSSUM (S'80–M'84–SM'91–F'98) is currently a Professor with the Thayer School of Engineering at Dartmouth. He is the primary inventor of the CMOS image sensor used in smartphones and other applications. He is currently exploring the quanta image sensor. He is the Co-Founder and the Past President of the International Image Sensor Society and a Director of the National Academy of Inventors. He was inducted into the National Inventors Hall of Fame and is a member of the National Academy of Engineering.